Article ID: 1006-8775(2018) 04-0494-14

A COMPARATIVE STUDY ON CHARACTERISTICS AND THERMO–DYNAMIC DEVELOPMENT MECHANISMS OF TWO TYPES OF WARM–SECTOR HEAVY RAINFALL ALONG THE SOUTH CHINA COAST

MIAO Chun-sheng (苗春生)[1], YANG Yi-ya (杨艺亚)[1, 2], WANG Jian-hong (王坚红)[1, 4], LI Ping (李 萍)[3]
(1. Collaborative Innovation Center on Forecast and Evaluation of Meteorological Disasters/ Key Laboratory of Meteorological Disaster, Ministry of Education, Nanjing University of Information Science & Technology (NUIST), Nanjing 210044 China; 2. Center for Monsoon System Research, Institute of Atmospheric Physics, Chinese Academy of Sciences, Beijing 100029 China; 3. Liaoning Meteorological Observatory, Shenyang 110016 China; 4. School of Marine Sciences, NUIST, Nanjing 210044 China)

Abstract: Warm-sector heavy rainfalls along the south China coast from April to June during 2009-2014 can be divided into two main types based on their low-level circulations. Type I is the southerly pattern with meridional convergence line at the west of the Pearl River estuary, which is formed by the convergence of southeasterly, southerly, and southwesterly flows. Type II is the southwesterly pattern with a latitudinal convergence line at the east of the Pearl River estuary, which is formed by the convergence of westerly and southwesterly flows. Statistics on 6-hourly heavy rainfall events indicates that, during the afore-mentioned 6 years, there were on average 73.2 occurrences of the southerly pattern and 50.3 occurrences of the southwesterly pattern per year. After the onset of summer monsoon in the South China Sea, the occurrence frequencies of both patterns increase remarkably. The synthetic diagnosis of pattern circulation shows that, at 500 hPa, for the southerly pattern, there is a broad warm high ridge, and a temperature ridge is behind the high ridge, which causes an obvious warm advection at the high ridge area. There is no frontal region. For the southwesterly pattern, the circulation is a weak trough with a temperature trough behind it. The position of the frontal region is near Yangzi River, and the south China coast is in the warm-sector of the frontal region. At the vertical cross-section of each of the two categories of heavy rainfall, there is a strong vertical motion center stretching to 400 hPa, where the convergence layer in the rainfall region is deep and with several vertical convergence centers overlapping one another. Both types of heavy rainfalls are with abundant water vapor, accompanied with deep convective instability energy layers, and with strong release of latent heat caused by condensation of water vapor. The release of latent heat leads to the warming-up and stretching of the air column, thus strengthens deep convergence and vertical velocity upward. There is a stronger latent heat-release in the southwesterly pattern than in the southerly pattern, while in the southerly pattern, the warm advection at middle and upper levels is stronger than the latent head release. To study the thermo-dynamic development mechanisms, weather research and forecasting model (WRF) numerical simulations are made and the results show that, in the two rainstorm regions, latent heat release warms up the air column, hence significantly increase the depth and strength of the vertical velocity. Moreover, the release of latent heat strengthens convergent circulation at lower levels and weakens divergent circulation at middle levels, whose influence can be as strong as 30%-50% of the wind circulation strength of the two types of the warm-sector heavy rainfall over the south China coast, and further enhances deep convection, promoting warm-sector storm development.

Key words: warm-sector heavy rainfall; the convergence line at low level; thermodynamic developing mechanism; numerical simulation; latent heat
CLC number: P47 **Document code:** A
doi: 10.16555/j.1006-8775.2018.04.008

1 INTRODUCTION

The Warm-sector Heavy Rainfall (WSHR) in south China occurs in the warm-sector at the south of the surface cold front, or in the case where there is no front between Nanling Mountains and the north region of the South China Sea, and south China is not controlled by a cold air mass or a property changing cold high. WSHR sometimes occurs at the convergence zone of southwest and southeast flow. When there is a cold front, heavy rainfall usually occurs 200–300 km south of the surface frontal zone (Huang et al.[1]; Tao[2]). Zhao et al.[3] demonstrated that WSHR is different from frontal heavy rainfall not only in aspects of instability type, dynamic and thermodynamic structure, but also in aspects of water vapor transport, mesoscale environment, and vertical circulation, which might account for the problems in

Received 2018 -02-23; **Revised** 2018-09-17; **Accepted** 2018-11-15
Foundation item: National Natural Science Foundation of China, "The Dynamic Structures and Maintaining Mechanisms of Oceanic Meso-scale Eddies" (41276033); National Natural Science Foundation of China Youth Science Fund Project "Research on Intelligent Identification, Forecast and Early-warning of Downburst" (41805033)
Biography: MIAO Chun-sheng, Professor, primarily undertaking research on multi-scale dynamics, meteorological information technology
Corresponding author: WANG Jian-hong, e-mail: jhwang@nuist.edu.cn

predictability and simulation of WSHR. The relationship between WSHR and other major synoptic systems has been well documented, Ding et al. analyzed the WSHR events occurred in May and June from 2005 to 2008 in south China and examined the relationship between WSHR and jet streams in the lower and upper troposphere as well as the South Asia High[4]. Wang et al. identified five heavy rainfall mode regions during the annually first raining season in south China by adopting the Rotated Empirical Orthogonal Function (REOF) method. Among these five regions, two regions in the south and north of Guangdong province receive higher precipitation rate and strength compared with the other regions (Wang et al.[5]). The mechanisms accounting for the heavy rain in these two regions are the cyclonic fronts or the frontogenesis in transformed field in the north region, and an orographic effect as the landfall of a subtropical system in the south region respectively. Chen et al. analyzed the synoptic systems responsible for the WSHR events in May and June for the period of 2000–2009, and categorized these synoptic systems into shearline-type, vortex-type and southerly-type [6]. Regarding the trigger of the south China WSHR, Ye et al. and Zhang et al. studied β meso-scale Mesoscale Convective System (MCS) as a trigger of the WSHR events in south China and its impact, the "train effect" due to successive outbreaks of MCS (Ye and Miao [7]; Zhang et al. [8]). Huang et al. suggested that there are various mechanisms responsible for WSHR in south China, and one of the important mechanisms is associated with gravity waves and inertia-gravity waves[1]. In addition, Maddox and Doswell evaluated the contribution from warm advection to the triggering of WSHR [9], and Meng et al. and Meng and Wang discussed the trigger effect of symmetric instability upon WSHR[10-11]. Gu et al., and Zhao et al. and Meng et al. focused on the heating effect due to latent heat release from precipitation and mid-level disturbance [12-14]. Lai et al. utilized numerical simulation to research into the accumulation of unstable energy near the surface, and water vapor effect transported via southwest jet streams[15]. It was well accepted in all these previous studies that WSHR possess characteristics include but not limited to the following: drastically disasters, various influence systems, complicated development mechanisms, and prediction difficulty.

Since WSHR has tropical system precipitation characteristics, its abundant water vapor content and thermodynamic trigger effect should be two crucial factors that sustain and enhance the heavy rain. In this article, we will perform classification statistical analysis and dynamic composition on the WSHR events happened in April-June between 2009 and 2014 in south China, as well as perform numeric simulations on typical examples of the two WSHR types, and further discuss the heavy rain characteristics of the two types of low-level convergence line in the warm-sector along the south China coast. We will also discuss the similarities and differences between the thermodynamic mechanisms of the two WSHR types. The results will provide a useful reference for forecasting and diagnosing the WSHR in south China. The role played by orography in WSHR, as well as the combined effect of orography and thermodynamics will be discussed in another paper.

2 DATA, CRITERIA AND CLASSIFICATION

South China is defined in this paper as a domain with a boundary of 105–120° E, 17–28° N. It includes Guangxi Zhuang Autonomous Region, Guangdong, Fujian and Hainan provinces. The coastal region is the focus of this study.

The datasets used in this study include National Centers of Environmental Prediction (NCEP) Final (FNL) analysis (1°×1°, 6-hourly), surface rain gauge data from surface stations and merged rainfall data (0.1°×0.1°) from automated weather observing systems in China and Climate Prediction Center Morphing (CMORPH) data which are produced with Climate Prediction Center (CPC) Morphing technique.

The following are the criteria used for our WSHR research: (1) since WSHR usually occurs during the annually first raining season in south China, we selected the months from April to June during the period of 2009–2014; (2) due to the fact that the WSHR-related precipitation mostly sustains only a few hours, we took each sample by measuring precipitations accumulated over a 6-hour window; (3) we adopted the definition of heavy rain, i.e., 6-hourly accumulated precipitation ≥25 mm; (4) as the WSHR in south China usually occurs in the warm-sector on the south of the surface front, which means it is controlled by the south China warm air mass, we defined the front as the area with very dense contour of near 850 hPa, and defined WSHR as heavy rain occurred 200-300 km to the south of the front or in the warm air mass if without a front.

According to the characteristics of the low latitude flows, we categorized the WSHR based on flow-field conditions in the lower levels, resulting in two types of convergence line based WSHR: (1) the southerly-type convergence line WSHR (S-WSHR), and (2) the southwesterly-type convergence line WSHR (SW-WSHR).

3 BASIC CHARACTERISTICS OF THE TWO TYPES OF WSHR IN SOUTH CHINA

3.1 *Statistical characteristics of the two types of convergence line based WSHR*

The composite map of 850 hPa flow field and 6-hourly accumulated precipitation for S-SWHR is shown in Fig.1a. In the lower levels, mainly due to the convergence of the southeasterly, southerly, and southwesterly flows, a north-facing longitudinal

convergence line is formed. In the annually first raining season, along the south China coast, especially to the west of the Pearl River estuary, heavy rain and localized heavy rain to extremely heavy rain usually happen because of such circulation pattern. The precipitation corresponding to S-WSHR has a short duration, usually within 6 hours, with a high concentration, i.e., usually 6-hour precipitation greater than 30 mm, or even greater than 40 mm. The rain zone is usually round-shaped with a scale from several tens of kilometers to several hundreds of kilometers, and it mostly occurs near Jiangmen or Yangjiang in Guangdong province. This type of WSHR often occurs when a transformed cold high weakens and moves out from the land towards the east to the sea. In this case, there is no front in south China, and the precipitation area is controlled by the warm air mass. Sometimes the southeasterly flow in the rear of the transformed cold high is very strong and it can bring abundant moisture to south China, resulting in heavy rain with distinctive returning flow characteristics.

SW-WSHR (Fig.1b), the second type of WSHR, is mainly caused by the convergence of westerly and southwesterly flows, forming a northeast-facing latitudinal convergence line, causing localized heavy storm to extremely heavy storm along the south China coast. SW-WSHR is often related to shearlines, low vortices and low-level jet streams near the coast. Its associated precipitation usually has a long duration: intermittent precipitation can last as long as over 10 hours, or even longer. The rain zone exhibits a narrow band and often covers an area from Pearl River estuary to the eastern coast of Guangdong province, stretching as far as a few hundred kilometers. The 6-hourly accumulated rainfall amount can be equal to or larger than 40 mm. It is common when a front is still above the southern Yangtze river while a very heavy rain has already started on south China coast (being far away from the Yangtze River by about five latitudes). Under such situation, the rain zone is in the unstable area with high-temperature, high-moisture on the south of the front. The low-level jet stream also plays an important role in this type of heavy rain. Strong southwesterly flow is obvious in the northwest of South China Sea and over Indochina Peninsula, and it is also exclusively the flow over the coast of south China. The flow over the north of the South China Sea is a low-level jet stream with the cyclonic shear on its left tends to cause and sustain SW-WSHR when happens along the south China coast.

Table 1 shows the statistics of the two types of WSHR for the period between 2009 and 2014 inclusively. There are 439 S-WSHR samples (sample is selected based on 6-hourly accumulated precipitation) and 302 SW-WSHR samples. There are in total more S-WSHR samples than SW-WSHR samples over the 6 years, which is also the case for each individual year, except for the year 2010. 2012 is the year of the most occurrences of S-WSHR, with 104 cases. On average, there are 73.2 S-WSHR cases and 50.2 SW-WSHR cases each year.

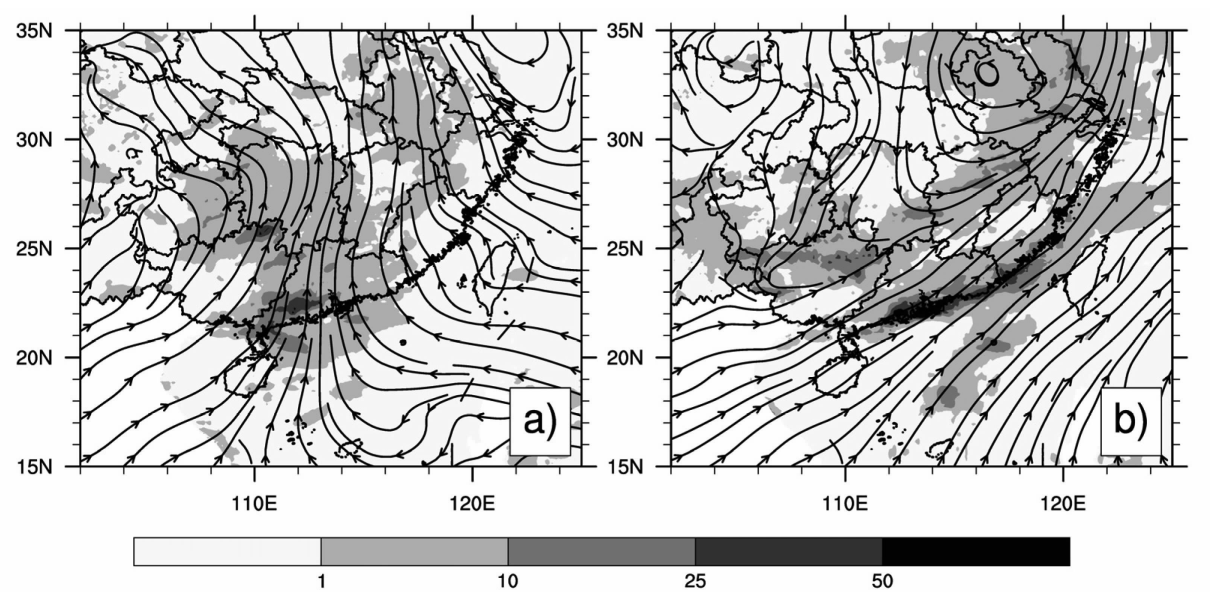

Figure 1. Composite 6-hourly accumulated precipitation and 850 hPa air flow field distribution for (a) S-WSHR and (b) SW-WSHR. Shading is precipitation based on the spectrum, unit: mm.

If we examine the monthly distribution of these two types of WSHR during the annually first raining season (the last three columns in Table 1), it is clear that the frequency of S-WSHR occurrence increases from April to June. In June, when usually the South China Sea monsoon occurs, the frequency of S-WSHR occurrence reaches the peak. The average number of S-WSHR occurrence in June is 33, which is about 42.9% of total S-WSHR occurrence during the annually first raining season. On the other hand, with the SW-WSHR, the most

active month is May, where average number of occurrences per year is 20.7, equivalent to 41% of all SW-WSHR occurrences during the annually first raining season. June is the second most active month for SW-WSHR, followed by April. The frequency of occurrence for both types of WSHR increases after the South China Sea monsoon becomes active.

Table 1. Statistics of the monthly and yearly distributions of samples for each type of WSHR during April-June, 2009-2014, unit: number of samples.

Year /Month	2009 (AMJ)	2010 (AMJ)	2011 (AMJ)	2012 (AMJ)	2013 (AMJ)	2014 (AMJ)	2009-14 April	2009-14 May	2009-14 June
S-WSHR	52	45	71	104	92	75	88	153	198
SW-WSHR	24	59	42	61	65	51	64	124	114
Total	76	104	113	165	157	126	152	277	312

3.2 *Composite characteristics of the two types of WSHR with convergence lines*

In this section, results from composite analysis of individual samples for each of the two types of WSHR are presented. The circulation pattern, adiabatic heating and development mechanisms are analyzed.

3.2.1 COMPOSITE DYNAMICS CHRACTERISTICS

Some distinct differences are evident between the composite 200 hPa streamline (figure not shown) maps for S-WSHR and SW-WSHR. The S-WSHR is in the right of the upper-level latitudinal jet stream, where the anticyclonic shear sustains the upper-level divergence through vertical pumping effect, which is favorable for enhancing the low-level flow ascending motion. The SW-WSHR, on the other hand, is controlled by the northwestern flow at the front of the anticyclone, whose wind speed is significantly less than that of S-WSHR However, the anticyclonic curvature is quite pronounced for SW-WSHR, indicating the intruding of cold and dry air mass from the north. With SW-SWHR, a front can be identified in the lower level, and south China is located at the warm-sector side of this front. However, the wind in the upper level is considerably weak, and the entire system exhibits weak baroclinicity. The composite geopotential height, wind and temperature fields at 500 hPa for the two types of WSHR are shown in Fig.2. For S-WSHR (Fig.2a), a broad warm ridge extends from northeast China to south China along the eastern coast of China, with south China at rear of the warm ridge. It also shows the temperature ridge lags the ridge of geopotential height, exhibiting obvious warm advection, with no front. For SW-WSHR (Fig.2b), there is a weak trough in the east of China. The temperature trough lags behind the trough of geopotential height. The front is near 30° N, hence south China is in the warm-sector of the front with weak low-level disturbance. The convergence line in the boundary layer of the flow field at 850 hPa is clear for both types of WSHR. The convergence line for S-WSHR is a south-facing longitudinal convergence line formed from flows from southwest, south, and southeast. It is usually located between the Pearl River estuary and Leizhou Peninsular. As for SW-WSHR, the converging flow is a latitudinal converge line comprised of western and southwestern flows, covering areas from the eastern part of Guangdong province to the southern part of Fujian province (Fig.1).

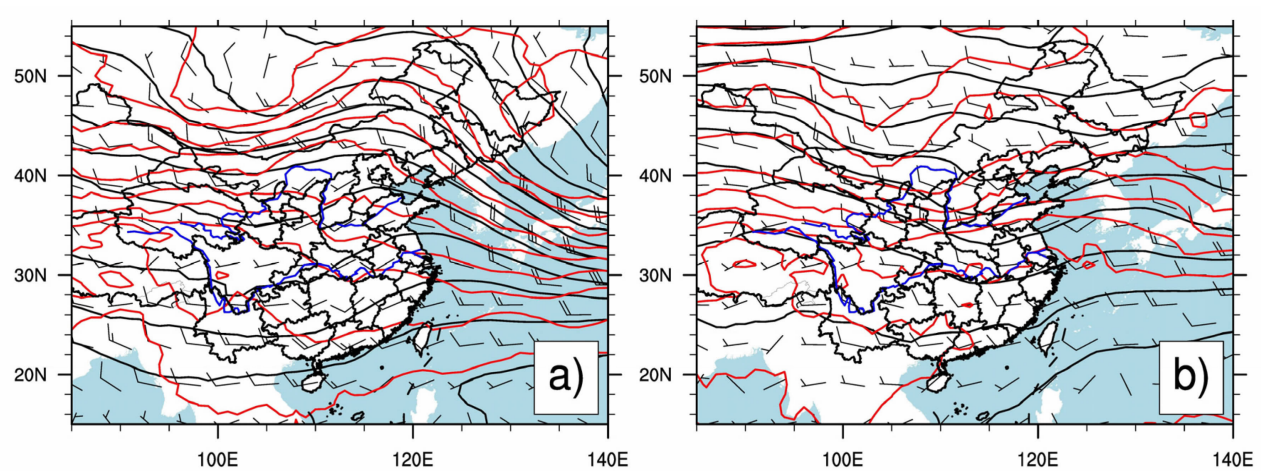

Figure 2. Composite geopotential height field (unit: gpm), wind field (unit: m/s), and temperature field (unit: ℃) at 500 hPa. (a) S-WSHR and (b) SW-WSHR.

By creating a longitudinal cross-section across the heavy rain center and depicting the vertical velocity on the cross section in each of the two types of WSHR, the following phenomena can be observed: For S-WSHR, the cross-section is at 112°E(Fig.3a); within the cross-section, there is a strong ascending motion within 20 –29° N, where there is a vertical motion center at 22°N extending from 850 hPa to 400 hPa and directly facing the heavy rain center on the west of the Pearl River estuary. The (v-w) circulation on the cross-section indicates that the air flow in the north of the South China Sea, on the south of 20° N, is flat and straight. Low-level climbing motion is weak. However, above the continent on the north of 20°N, the air flow climbing motion becomes distinctively stronger, which should be associated with the mountain upraising effect, the suction effect caused by divergence of middle and high circulations, as well as condensation latent heat generated from vertical transport of water vapor. On the other hand, for SW-WSHR, the cross-section is at 113°E (Fig.3b), and a vertical motion center is at 22 °N in the cross-section. In this cross-section, the ascending region corresponding to the heavy rain center covering the south China coast on the east of the Pearl River estuary exhibits the strongest vertical motion, and this region appears in the middle and upper levels. The (v-w) circulation for the vertical motion center at 22°N has dominant vertical composition, located in the heavy-rain region circulation vertical direction, and inclines southward to the heavy-rain region, resulting in a vertical secondary circulation, which is strong but unstable. The formation of ascending motion center should be associated with increased vertical traction of air columns caused by the combined effect of lateral orographic friction, low-level systematic convergent rising, upper-level anticyclonic divergent suction effect, as well as the release of condensation latent heat. Since the vertical motion happens in an elevated position, the release of condensation latent heat contributes more to the formation of the motion center in the warm-sector.

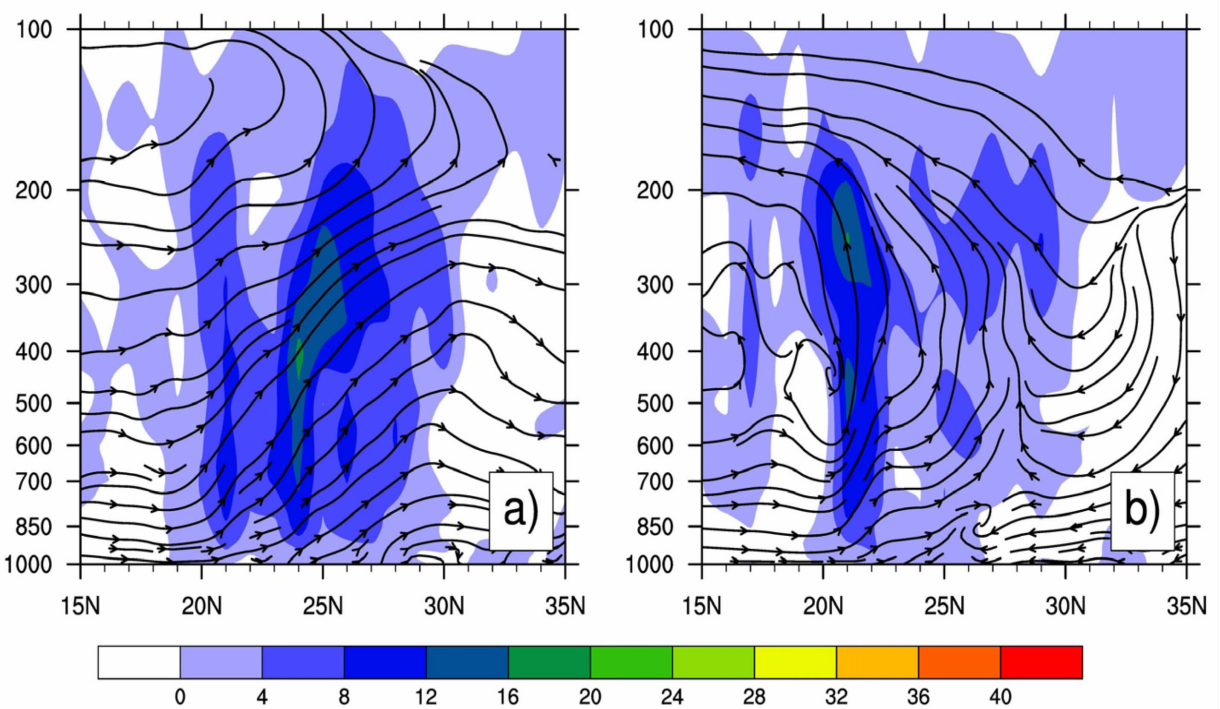

Figure 3. The longitudinal cross-sections of vertical distribution and vertical velocity of circulations for (a) S-WSHR, cross-section at 112° E and (b) SW-WSHR, cross-section at 113° E. Shading represents vertical velocity, and solid line represents v-w composite streamline, unit: m/s.

The characteristics of the vorticity and divergence on the latitudinal vertical cross-sections of the two types of WSHR are depicted in Fig.4. For S-WSHR (Fig.4a), 112° E is the center of the heavy rain, where in the lower levels there is a convergence center and a positive vorticity center. An even stronger positive vorticity center appears at around 600 hPa, which is favorable for sustaining a low-pressure system and strong upward motion. A layer of strong convergence reaching up to as high as 500 hPa is over the area of heavy rainfall. Several vertically overlapped centers of convergence are at 1,000 hPa, 850 hPa and 600 hPa (contour for divergence not displayed to clearly display positive vorticity and contour for convergence). In comparison, for SW-WSHR, the center of heavy rainfall is between 112–115° E. There are also convergence centers and positive vorticity centers corresponding to SW-WSHR at the lower levels. In contrast to the rounded rain zone of S-WSHR, the

precipitation associated with SW-WSHR exhibits rather a latitudinal band shape. Compared with S-WSHR, WS-WSHR has a deeper layer of convergence and a larger positive vorticity, reaching up to 400 hPa and above. The magnitudes of both vorticity and divergence are larger than those of the S-WSHR type. There are more vertically overlapped centers of convergence in WS-WSHR, located at 1,000 hPa, 850 hPa, 600 hPa, 400 hPa and 300 hPa, which is helpful to sustain vigorous upward motion over the heavy rain. In general, both WSHR types have strong low-pressure system, especially at vertically overlapped convergence centers. Such phenomenon reflects different influences imposed by dynamic and thermodynamic mechanisms, including low-level orography and circulation dynamics as well as upper-level condensation latent heat mechanisms.

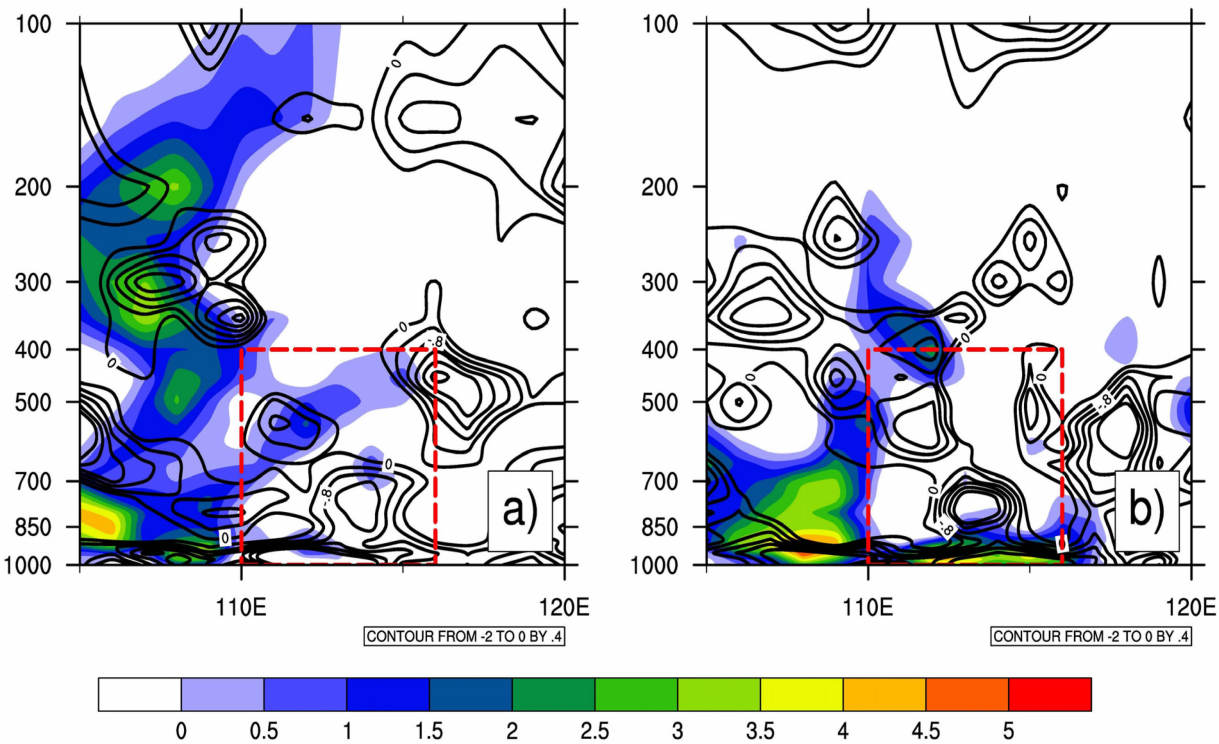

Figure 4. The latitudinal vertical cross-sections of composite relative vorticity (shadings, unit: 10^{-5}/s) and divergence (contour, positive divergence not shown, unit: 10^{-5}/s) along 22°N for (a) S-WSHR and (b) SW-WSHR.

3.2.2 COMPOSITE CHARACTERISTICS OF ADIABATIC HEATING

The WSHR in south China occurs at the boundary between land and sea where moisture is abundant. The water vapor is vertically transmitted through upward dynamic motion and condenses at upper troposphere over the area of heavy rain, which results in strong adiabatic heating. Adiabatic heating Q includes apparent heat source Q_1 and apparent moisture sink Q_2. Q_1 represents temperature increase of unit mass air during unit time, Q_2 represents rate of temperature increase due to condensation latent heat release of unit mass moist air during unit time. Their formulas are shown below

$$Q_1=C_p[\frac{\partial T}{\partial t}+V\cdot\nabla T+\left(\frac{p}{p_0}\right)^{R/C_p}\omega\frac{\partial\theta}{\partial p}] \quad (1)$$

$$Q_2=-L[\frac{\partial q}{\partial t}+V\cdot\nabla q+\omega\frac{\partial q}{\partial p}] \quad (2)$$

where C_p is specific heat under constant pressure, q is specific humidity and L is latent heat. According to formulas (1) and (2), Q_1 results from the local changes in temperature and advection, Q_2 results from changes in condensation latent heat release.

The adiabatic heating profiles at the centers of heavy rainfall for both types of WSHR are shown in Fig.5. For S-WSHR, Q_1 is larger than Q_2 above 900 hPa, indicating heating due to warm advection associated with the warm ridge is dominant over condensation latent heat release. In contrast, the larger Q_2 below 900 hPa reflects that heating due to latent heat release associated with orographic climbing effect is dominant. It is also necessary to mention that vertical variation of Q_2 is negligible at mid-level but pronounced at lower and upper levels. For SW-WSHR, adiabatic heating stays positive up to 500 hPa. Both Q_1 and Q_2 heat the air, but generally Q_2 is larger than Q_1, indicating heating due to latent heat release is more prominent in the middle and upper levels for SW-WSHR. Below 900 hPa, the warm advection corresponding to the confluence flow from the ocean plays a dominant role.

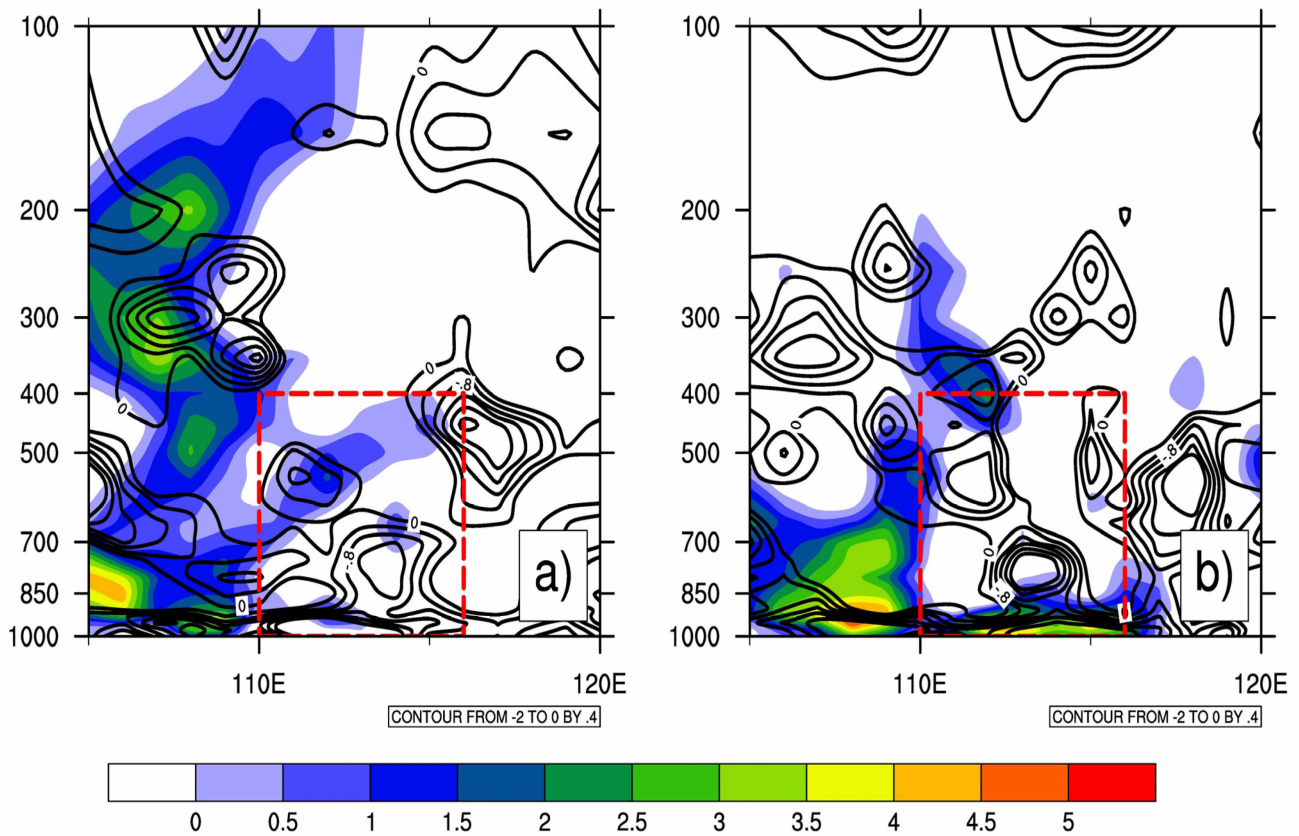

Figure 5. Composite profiles of apparent heat source Q_1 and apparent moisture source Q_2 at the center of heavy rainfall for (a) S-WSHR and (b) SW-WSHR (unit: 10^{-3} J /(kg·s)).

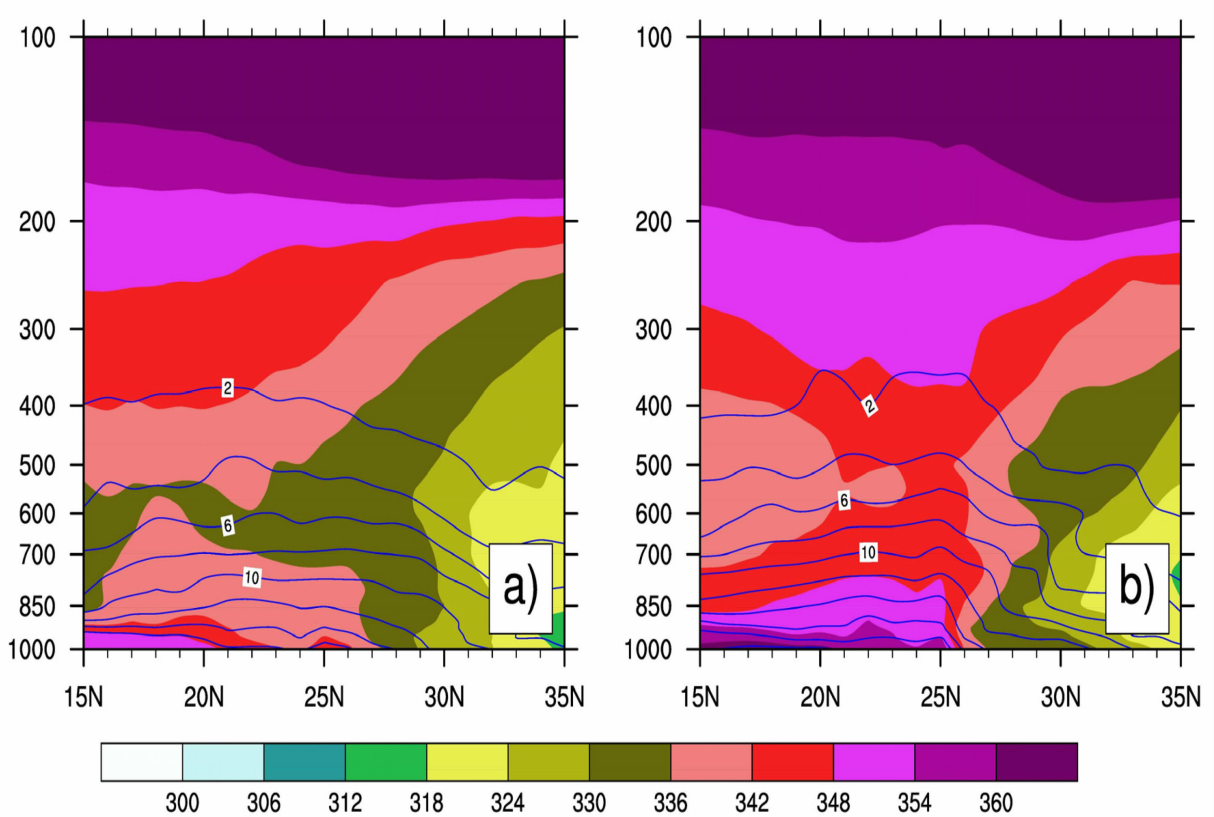

Figure 6. Longitudinal vertical cross-sections of composite pseudo-equivalent potential temperature θ_{se} (shading, unit: K) and specific humidity (unit: g/kg) for (a) S-WSHR along 112°E and (b) SW-WSHR along 113°E.

3.2.3 COMPOSITE CHARACTERITICS OF CONVECTIVE INSTABILITY

Environmental convection is considered unstable if pseudo-equivalent potential temperature decreases with altitude. For S-WSHR (Fig.6a), within the area of heavy rain on the south China coast (south of 25° N), θ_{se} decreases with altitude (color spectrum in Fig.6a) within a deep convective unstable layer (up to 500 hPa). The low-level gradient of unstable stratification is even larger at the center of heavy rain which is around 22° N. The stratification is stable on the north of 27° N where θ_{se} increases with altitude. The cross-section of composite specific humidity shows a moist tongue near the center of heavy rain, indicating abundant moisture in the heavy rain zone. The thickness of the moist tongue is greater than the thickness of the moist air to the south and north of the heavy rain zone. The specific configuration of convective unstable energy and centralized abundant moisture source is favorable for sustaining very heavy rainfall. For SW-WSHR, like S-WSHR, it also shows θ_{se} decreases with altitude (shades based on color spectrum) on the south of 25° N, and extends to 600 hPa, maintaining a reasonably deep convective unstable layer. The stratification on the north of 25° N for SW-WSHR is slightly unstable at lower levels, but becomes stable above 850 hPa, where θ_{se} increases with altitude. A moist tongue penetrating up to 400 hPa is evident near the center of heavy rain (22° N). The vertical gradient and magnitude of specific humidity for SW-WSHR are both larger than those for S-WSHR, implying a better moisture condition and the existence of stronger unstable energy.

As is analyzed above, both S-WSHR and SW-WSHR have abundant moisture and a deep convective unstable layer. Therefore, a large amount of latent heat is available for both types, which promotes the formation of a warm core system over the area of heavy rainfall, the maintenance of an air column tensile low-pressure system, as well as rigorous convergent and ascending air flows. However, there are still differences between these two types of WSHR in terms of basic characteristics and formation mechanisms due to differences in factors such as typical circulation structure, e.g. convergence line as well as the role played by orography (blocking, lateral friction, and dynamic lifting). To investigate the composite dynamic and thermodynamic effects, it is necessary to divide the research into two parts: the first part is to examine the combined effects of thermodynamics and circulation dynamics, which is the focus of this paper. The second part is to study the combined effects of thermodynamics and orographic dynamics, which will be discussed in a separate paper.

4 THERMODYNAMIC MECHANISM OF WSHR

The Weather Research and Forecasting (WRF) model is used to study the thermodynamic mechanism of WSHR.

4.1 *Results of controlled tests and thermodynamic experiment schemes*

The WRF v3.5 mesoscale model is employed in this study. We selected two typical cases from each of these two types of WSHR samples to simulate and experiment with. Triple nested grid is applied to both controlled experiments (Test of Control: TCTL), the grid resolution setting is: 36 km for D01, 12 km for D02, and 4 km for D03. The simulation period for the typical case of S-WSHR is 12Z (UTC, same hereafter) May 7−12Z May 8, 2013. The selected physical process schemes include but not limited to (1) WRF Single-Moment 3-Class Microphysics Scheme (WSM3) microphysics process; (2) Cumulus Troposphere Parameterization Scheme: Kain-Fritsch used for D01, Betts-Miller-Janjiéĉé (BMJ) used for D02 and no cumulus process considered for D03; (3) Yonsei University (YSU) Scheme, used for planetary boundary layer; (4) Rapid Radiative Transfer Model (RRTM), etc. For SW-WSHR, the simulation period is 06Z May 21-12Z May 22, 2013. The parameterization schemes are same with those used in S-WSHR type, except that the microphysics scheme used is the Ferrier scheme. Fig.7 shows the results of TCTL experiments.

By comparing the actual observations and TCTL results of the two types of WSHR, we can conclude that the location of the rainfall, shape of the rain band as well as the center of the heavy rainfall are well simulated in TCTL experiments. In addition, the tempo-spatial distribution of precipitation rate, vertical velocity, and the magnitude of the latent heat release all align with the observations very well, space-wise, and time-wise. For instance, when the released latent heat reaches the maximum at mid-upper level, the corresponding vertical velocity is also the largest with the longest duration. The latent heat release in SW-WSHR is much stronger and has longer duration than that in S-WSHR. Therefore, the verification of TCTL experiments justified the selected parameterization schemes and the initial boundary conditions.

To analyze the thermodynamic effects of latent heat, we designed a few sensitivity experiments (Test of Removal Latent Heat: RML). In RML experiments, the latent heating and the cumulus convection are switched off, while other parameterization schemes are kept the same as TCTL experiments.

4.2 *Two types of condensation latent heating*

Compared with the rainfall pattern in TCTL experiments, the distributions of the simulated rainfall in RML experiments for S-WSHR and SW-WSHR are considerably scattered. The precipitation rate and rainfall area are both reduced, and the 24-hourly, 12-hourly, and 6-hourly accumulated precipitation are all significantly decreased.

Figure 8 depicts the cross-sections of temperature difference between TCTL and RML experiments along

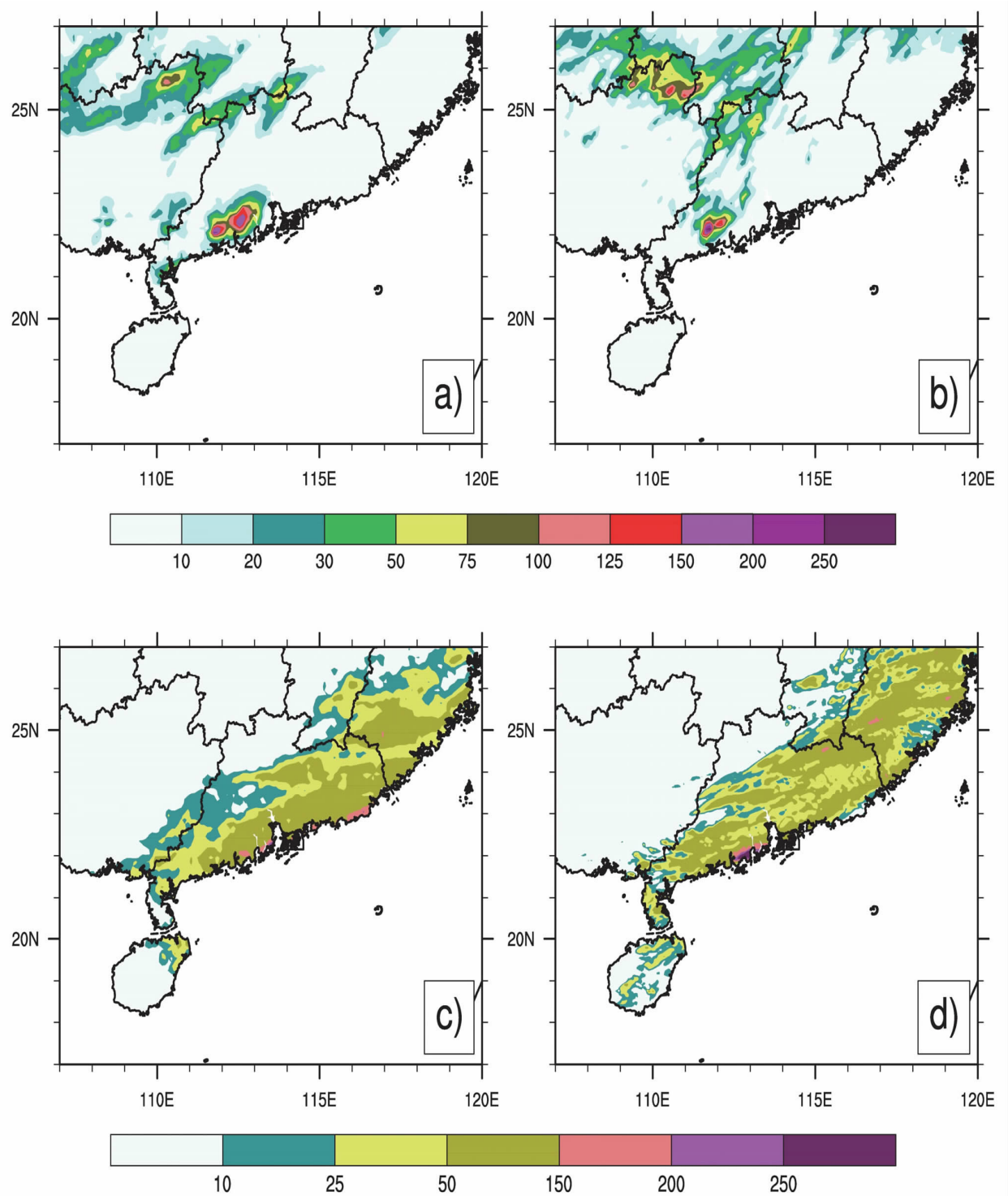

Figure 7. A comparison between simulated precipitation in TCTL experiments and actual observed precipitation for S-WSHR (a, b) and SW-WSHR (c, d) (unit: mm).

the longitude passing the center of heavy rainfall. Fig. 8a-8c is cross-sections captured at 00Z, 03Z and 04Z May 8, 2013 along 111.8° E for S-WSHR. For the center of heavy rainfall near 22°N, it coincides with the converging flow landfall orography. The warming can be noticed for the whole layer, indicating remarkable heating of the air column by the latent heat release. Multiple warming centers can be found over the mountainous terrain around 22°N, where the warming is most significant at 400 hPa. During the heavy rainfall, the heating increases with time, and it reaches maximum at 03Z, with a temperature increase as high as 6℃. Especially, as the thickness of the air column increases (Fig.8b), it expands from the surface of the orography up to almost 250 hPa. By 04Z, the

warming due to latent heat release decayed, both the warming rate and the thickness of the air column decreased. The results support the argument that warming due to latent heat release can cause the stretching of air column which will enhance and sustain the low-pressure system, which is favorable for a deep system structure of low-level convergence and upper-level divergence, speeding up upward motion. In the meantime, the warming centers at different heights in the air column also help to sustain the vertically overlapped convergence centers in the air column. Such effect resembles the Conditional Instability of Second Kind (CISK) mechanism in the formation of a typhoon. The peak time of warming corresponds to the time of most intense precipitation. The precipitation dissipates quickly when the warming due to latent heat release decays, indicating the important role played by latent heat release in mechanisms in developing and sustaining heavy rainfalls.

Figure 8d-8f presents the cross-sections of temperature difference along 113° E between TCTL and RML experiments captured at 18Z, 22Z and 23Z on May 21, 2013 for SW-WSHR. For the center of heavy rainfall near 22-23° N, the warming due to latent heat release mainly occurs between 850 hPa and 250 hPa. Unlike the distinct orographic uplifting effect in S-WSHR, the terrain does not have substantial impact on heavy rainfall for SW-WSHR. This is probably because the low-level air flow movements relative to the coastal mountains are mostly lateral flows around the mountains. The warming due to latent heat release reached a maximum of around 5℃ in temperature increase at 22Z between 500 hPa and 400 hPa (Fig.8e). Compared with 18Z, both the warming strength and the warming thickness of the air column at the center of the heavy rainfall are obviously enhanced and increased at 22Z. The intense rainfall started to dissipate after the weakening of the latent heat warming at 23Z.

Corresponding to the large vertical ascending

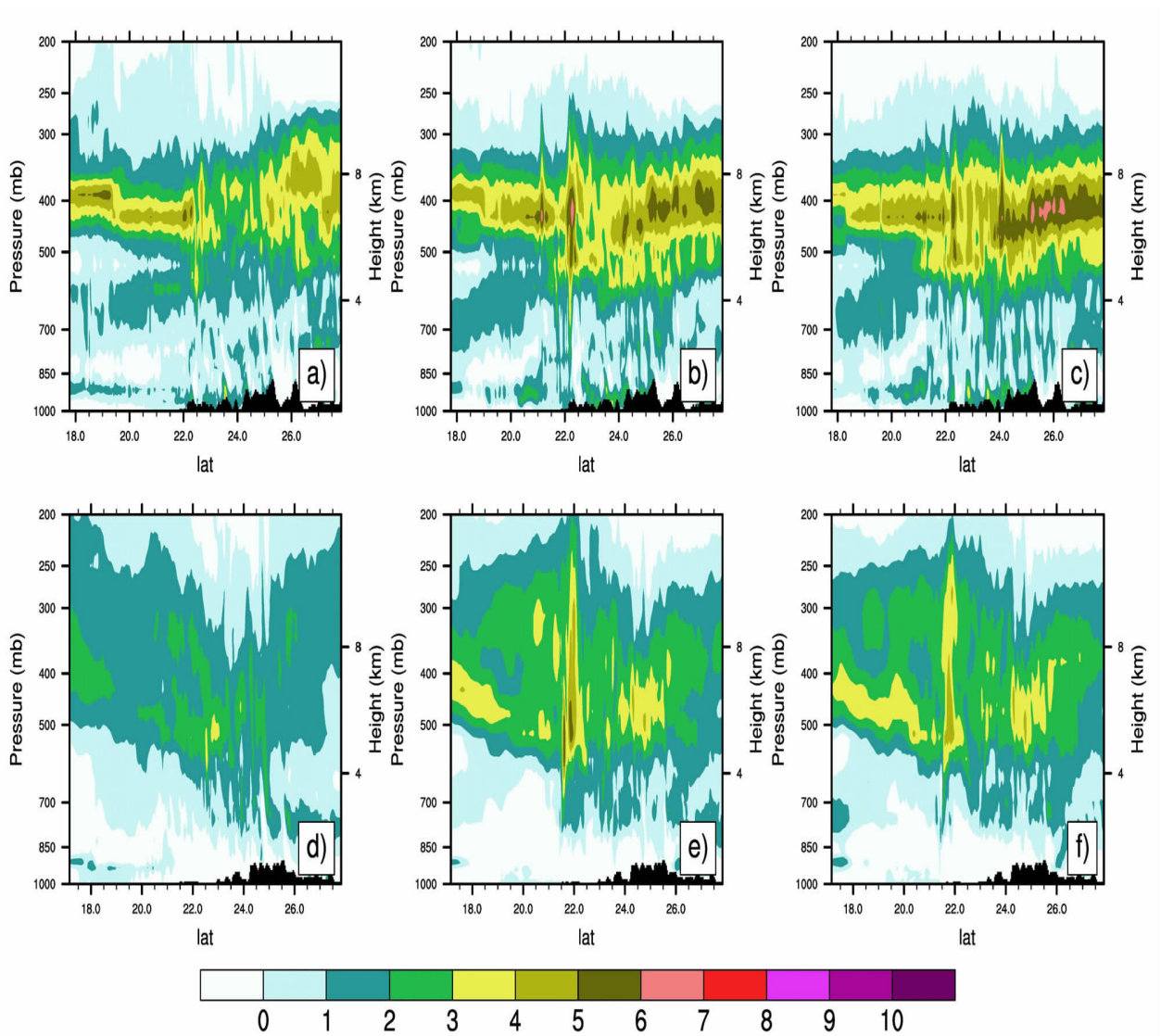

Figure 8. Longitudinal vertical cross-sections of composite temperature difference between TCTL and RML experiments at three simulation moments for S-WSHR (a-c) along 118°E at 00Z, 03Z, 04Z on May 8, 2013 and for SW-WSHR (d-e) along 113°E at 18Z, 22Z, 23Z on May 21, 2013 (unit: ℃).

velocity and strong vertical transport of water vapor, during the heavy rain, the warming of the air column also helps to maintain the vertically overlapped convergence centers. These facts imply the positive contribution of latent heat release to the warming of the air column, the deepening of the low-pressure system and the sustaining of vigorous vertical motion, which highlights the crucial role played by condensation latent heat in the mechanisms accounting for the initiation and advancement of the heavy rainfall.

4.3 *Impacts of latent heat release on circulations at different levels*

4.3.1 IMPACTS ON LOW-LEVEL CIRCULATIONS AT 850 hPa

Figure 9 shows the differences between wind vectors at 850 hPa in TCTL experiment which includes latent heat release and wind vectors at 850 hPa in RML experiments which removes latent heat release. The figures showing the difference fields of wind vectors for S-WSHR (Fig.9a) and SW-WSHR (Fig.9b) both correspond to the time when the heaviest rainfall occurred, as shown in Fig.8b (S-WSHR) and Fig.8e (SW-WSHR). The vectors shown in Fig.9 represent the wind vector difference (deviation wind), and the thin solid contour represents the wind speed difference.

As is shown in Fig.9a, in the rain zone for S-WSHR, i.e., near 112° E along the coast, the deviation wind is convergent. A positive wind speed difference center is also visible with the difference at 4 m/s. This means latent heat release enhances the low-level convergent circulation flow field. Because the range of the wind speed for the RML experiment within the domain of this figure is 4-8 m/s, the acceleration of wind caused by latent heating can be more than 50%. Like the impact on S-WSHR, the influence of latent heat on SW-WSHR (Fig.9b) is reflected in convergent deviation winds along the coast of south China between 113°E and 116°E, with a 4 m/s positive wind speed difference contour encircling an area including the coastal heavy rainfall area and its adjacent ocean. This reveals the contribution from latent heat to low-level flow field convergence and to the acceleration of moisture transport, as well as to the enhancement of low-level jet streams. For SW-WSHR, the range of wind speeds for the experiments without latent heat release is 8-14 m/s, thus the acceleration of wind caused by latent heat can be over 30%.

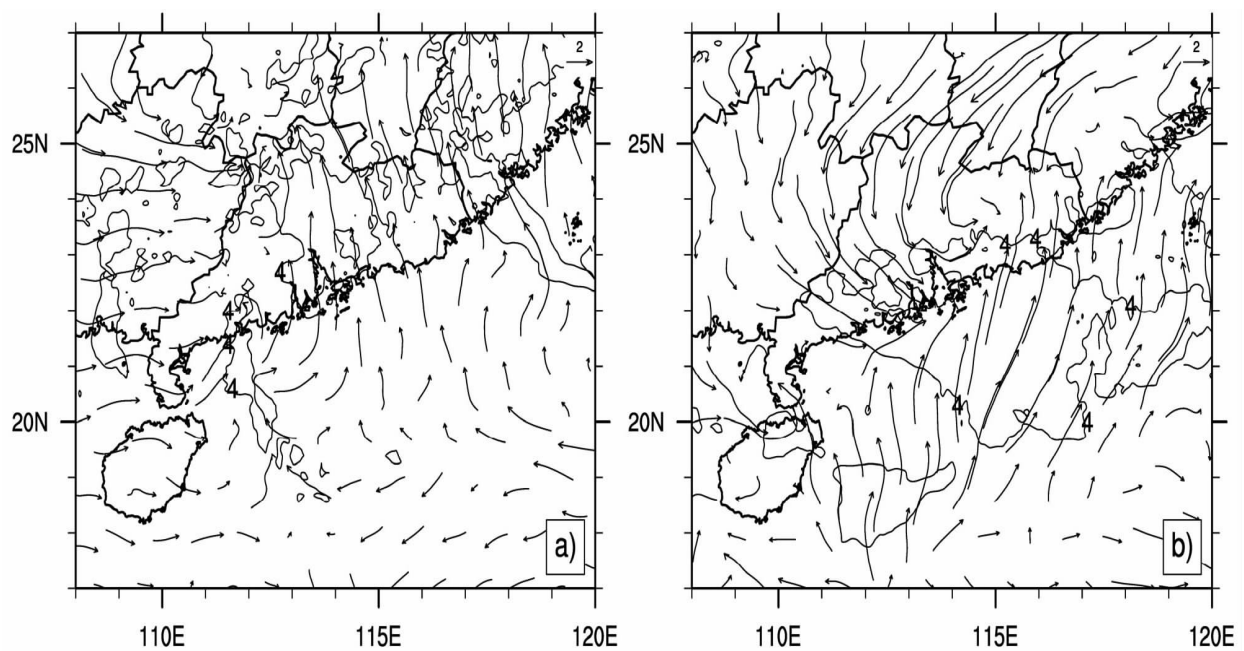

Figure 9. Differences of 850 hPa wind during the heaviest rain between TCTL and RML experiments for (a) S-WSHR (at 03Z May 8 2013) and (b) SW-WSHR (at 22Z May 21 2013). (unit: mm, vectors and contours represent the wind vector difference and wind speed difference respectively).

4.3.2 IMPACTS ON MID-UPPER LEVEL CIRCULATIONS AT 400 hPa

The differences between wind vectors at 400 hPa in TCTL experiment and wind vectors at 400 hPa in RML experiment are depicted in Fig.10. Like Fig.9, these plots correspond to the time when the heaviest rainfall occurred. For S-WSHR, as Fig. 10a presents, in the heavy rain zone, i.e., near 112°E along the coast at 400 hPa, the wind vector differences are divergent with a center of negative wind speed difference of −6 to −8 m/s. This indicates that latent heat does help maintain a divergent circulation at mid-level troposphere but decelerates the winds. As the condensation latent heat heating center exists around 400 hPa (Fig.8b), the heating leads to a decrease of pressure at the corresponding level and indicates the development of a low-pressure system. The

strength of divergence decreases, so does the divergent wind speed, which causes the vertical thickness of the system increases. The range of wind speed is about 14-20 m/s in the experiments without latent heat release, thus the decrease of the mid-level divergent wind speed caused by latent heat can be over 40%. For SW-WSHR (Fig.10b), the impact of latent heat release is similar with that in S-WSHR. The deviation wind at 400 hPa level over the area of heavy rainfall near 113-116° E is also divergent, with a center of negative wind speed difference of −4 to −6 m/s along the coast. The latent heat release again sustains a divergent circulation at mid-level troposphere but decelerates the wind speed. Same as with S-WSHR, as the condensation latent heat heating center exists around 400 hPa, the heating leads to a decrease of pressure at the corresponding layer and indicates the development of a low-pressure system. The strength of divergence decreases, so does the divergent wind speed. The range of wind speed is about 14-20 m/s in experiment without latent heat release, thus de-acceleration of wind caused by latent heat is over 30%.

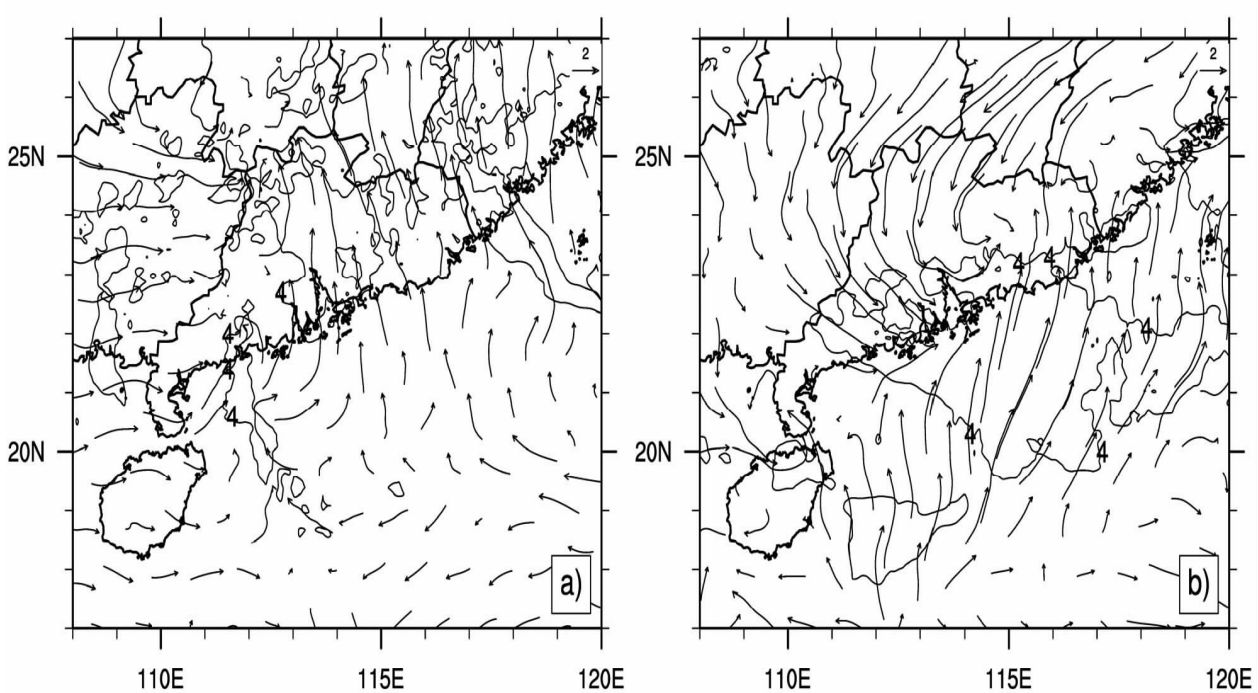

Figure 10. Differences of 400 hPa wind during the heaviest rain between TCTL and RML experiments for (a) S-WSHR (at 03Z May 8, 2013) and (b) SW-WSHR (at 22Z May 21, 2013). (unit: mm, vectors and contours represent the wind vector difference and wind speed difference respectively) (Same as Fig. 9, except for 400 hPa instead of 850 hPa).

Apparently, WSHR occurs in an environment where abundant moisture is available, which makes it possible for sufficient latent heat release. The latent heat warms the air column, enhances, and maintains a deep low-pressure system as well as the thickness and intensity of a strong upward motion layer of the low-pressure system. Furthermore, latent heat release enhances the low-level convergence and weakens mid-level divergence by 30%-50%, substantially facilitates the development of WSHR. To conclude, given abundant moisture, latent heat release affects the dynamic variables and the mid-lower-level circulation through thermodynamic heating effects, which is one of the important mechanisms for initiating and advancing WSHR.

5 CONCLUSION AND DISCUSSION

Through statistical analysis, composite diagnosis, and numerical simulation, the characteristics of WSHR occurred near the south China coast are investigated, and the thermodynamic mechanisms responsible for WSHR are summarized. The following are the conclusions:

(1) Based on low-level convergence lines, WSHR in south China can be divided into two types: the first is the WSHR with a southerly-type convergence line and mainly located at the west of Pearl River estuary (S-WSHR) which is characterized by a converging flow consists of southwest, south and southeast flows, forming a north-south orientated convergence line; the second is the WSHR with a southwesterly-type convergence line and mainly located at the east of Pearl River estuary (SW-WSHR), which is characterized by a converging flow consists of south and southwest flows, forming a southwest-northeast orientated convergence line.

(2) According to the characteristics of these two types of WSHR revealed by statistics, S-WSHR usually has a rounded-shape rain zone, and it often occurs in Yangjiang and Jiangmen of Guangdong province. The heavy rain associated with S-WSHR usually has a short

duration with a large precipitation rate. The rain zone is controlled by warm air mass, and no front is present in south China. SW-WSHR often occurs in the area between the Pearl River estuary and the coast of eastern Guangdong province, with a long duration of heavy rainfall. The rain zone usually has a narrow band shape, and is in the area with high temperature, abundant moisture, unstable stratification, and strong low-level jet flow. Based on statistics of 6-hourly accumulated precipitation samples, there is on average 73.2 events/year of S-WSHR and 50.3 events/year of SW-WSHR for 2009-2014. The occurrences of both types of WSHR increase significantly after the outbreak of South China Sea summer monsoon.

(3) Composite analysis shows remarkable differences between these two types of WSHR. For S-WSHR, there is a broad warm ridge over east China at 500 hPa, and south China is at the rear of the warm ridge. As the temperature ridge lags behind the ridge of geopotential height, there is substantial warm advection over south China, and no front there. For SW-WSHR, there is a weak trough over east China at 500 hPa, and the mid-latitude temperature trough lags behind the trough of geopotential height. A front zone can be found on the north of 30° N. South China is controlled by warm air mass on the south of the front where weak disturbances are evident. The weather system accounting for WSHR is a strong low-pressure system with vigorous upward motion in the cross-sections over the area of heavy rainfall, and the center of upward motion can reach 400 hPa and 250 hPa for S-WSHR and SW-WSHR respectively. Strong convergence is evident over the area of heavy rainfall, which is represented by multiple vertically overlapped convergence centers. The vertical convergent structure reflects different contributions from dynamic and thermodynamic effects, including the dynamic interaction between orography and surface circulation as well as thermodynamic effect of the latent heat release at upper levels.

(4) There are abundant moisture and a strong unstable stratification for both types of the WSHR. Therefore, a large amount of latent heat is released which is favorable for the development of a warm core system. The air column stretches due to latent heating, which maintains the intensity of the low-pressure system as well as the strong convergent upward motion of the air flow. The latent heat release in SW-WSHR is more prominent than that in S-WSHR. In S-WSHR, heating due to warm advection at mid-upper level is predominant over latent heat release.

(5) Results from numerical simulations reveal that abundant moisture is available for both types of WSHR, which provides a sufficient environment for a large amount of latent heat release. Latent heat release warms the air and leads to the stretching of the air column, which helps maintain a deep low-pressure system and the intensity and thickness of its corresponding vigorous upward motion. In addition, latent heat release also facilitates the development of WSHR by enhancing low-level convergence and weakening mid-level divergence by 30% −50% . Therefore, with abundant moisture available, latent heat release can enhance dynamic conditions through thermodynamic effect, and further improve low-level circulation, which is one of the important development mechanisms for WSHR.

The orographic effect and the combined effect of thermodynamic effect and dynamic forcing due to orography will be discussed in another paper.

REFERENCES:

[1] HUANG Shi-song, LI Zhen-guang, BAO Cheng-lan, et al. The Annually First Rainy Season over Southern China [M]. Guangzhou: Guangdong Technology Press, 1986: 227-228 (in Chinese).

[2] TAO Shi-yan. Chinese Rainstorms [M]. Beijing: Science Press, 1980: 225 (in Chinese).

[3] ZHAO Yu-chun, LI Ze-chun, XIAO Zi-niu. Comparison analysis of south China front and warm-area heavy rain systems in June 2006 [J]. Meteor Sci Technol, 2008, 36(1): 47-54 (in Chinese).

[4] DING Zhi-ying, LIU Cai-hong, SHEN Xin-yong. Statistical analysis of the relationship among warm-sector heavy rainfall, upper and lower troposphere jet stream and South Asian High in May and June from 2005 to 2008 [J]. J Trop Meteor, 2011, 27(3): 307-316 (in Chinese).

[5] WANG Jian-hong, XU Bi-yu, LIU Gang, et al. Dynamic characteristics of rainstorm division in Guangdong province and analysis of a severe rainstorm process [J]. J Meteor Environ, 2014, 30(6): 43-51 (in Chinese).

[6] CHEN Xiang-xiang, DING Zhi-ying, LIU Cai-hong, et al. Statistical analysis on the formation system of warm-sector heavy rainfall in May and June from 2000-2009 [J]. J Trop Meteor, 2012, 28(5): 707-718 (in Chinese).

[7] YE Lang-ming, MIAO Jun-feng. Mesoscale analysis of a typical heavy rain event caused by returning flow in the warm-sector in southern China [J]. Torr Rain Disast, 2014, 33(1): 342-350 (in Chinese).

[8] ZHANG Xiao-mei, MENG Wei-guang, ZHANG Yan-xia, et al. Analysis of mesoscale convective systems associated with a warm sector heavy rainfall event over south China [J]. J Trop Meteor, 2009, 25(5): 551-560 (in Chinese).

[9] MADDOX R A, DOSWELL C A III. An examination of jet stream configurations, 500 mb vorticity advection and low-level thermal advection patterns during extended periods of intense convection [J]. Mon Wea Rev, 1982, 110 (3): 184-197.

[10] MENG Wei-guang, WANG An-yu, LI Jiang-nan, et al. Moist potential vorticity analysis of the heavy rainfall and mesoscale convective systems in south China [J]. Chin J Atmos Sci, 2004, 28(3): 330-341 (in Chinese).

[11] MENG Wei-guang, WANG An-yu, LI Jiang-nan, et al. Multi_MCSs (Mesoscale Convective Systems) over the heavy rainfall region during 23-24 May 1998 in south China [J]. Acta Sci Nat Univ Sunyatseni, 2003, 42 (3): 73-77 (in Chinese).

[12] GU Chi-ming, FENG Ri-quan, WU Chi-sheng, et al. A

modeling case study of heavy rain event over south China in May 1994 [J]. J Trop Meteor, 2000, 16(2): 173-179 (in Chinese).

[13] ZHAO Yu-chun, WANG Ye-hong, CUI Chun-guang. A PV inversion diagnosis and numerical research on an extreme heavy rain in southern China flooding season [J]. Torr Rain Disast, 2008, 27(3): 193-203 (in Chinese).

[14] MENG Wei-guang, ZHANG Yan-xia, DAI Guang-feng, et al. The formation and development of a heavy rainfall mesoscale convective system along southern China coastal area [J]. J Trop Meteor, 2007, 23(6): 521-530 (in Chinese).

[15] LAI Shao-jun, HE Fen, CHEN Hai-shan, et al, Numerical simulation and diagnostic analysis of a rainstorm during the annually first rainy season of south China [J]. J Trop Meteor, 2012, 28(3): 409-416 (in Chinese).

Citation: MIAO Chun-sheng, YANG Yi-ya, WANG Jian-hong, et al. A comparative study on characteristics and thermo- dynamic development mechanisms of two types of warm-sector heavy rainfall along the south China coast [J]. J Trop Meteor, 2018, 24(4): 494-507.